nature neuroscience

Spontaneous activity regulates Robo1 transcription to mediate a switch in thalamocortical axon growth

Erik Mire[1,7], Cecilia Mezzera[1,7], Eduardo Leyva-Díaz[1], Ana V Paternain[1], Paola Squarzoni[2–4], Lisa Bluy[1], Mar Castillo-Paterna[1], María José López[1], Sandra Peregrín[1], Marc Tessier-Lavigne[5,6], Sonia Garel[2–4], Joan Galcerán[1], Juan Lerma[1] & Guillermina López-Bendito[1]

Developing axons must control their growth rate to follow the appropriate pathways and establish specific connections. However, the regulatory mechanisms involved remain elusive. By combining live imaging with transplantation studies in mice, we found that spontaneous calcium activity in the thalamocortical system and the growth rate of thalamocortical axons were developmentally and intrinsically regulated. Indeed, the spontaneous activity of thalamic neurons governed axon growth and extension through the cortex *in vivo*. This activity-dependent modulation of growth was mediated by transcriptional regulation of Robo1 through an NF-κB binding site. Disruption of either the *Robo1* or *Slit1* genes accelerated the progression of thalamocortical axons *in vivo*, and interfering with Robo1 signaling restored normal axon growth in electrically silent neurons. Thus, modifications to spontaneous calcium activity encode a switch in the axon outgrowth program that allows the establishment of specific neuronal connections through the transcriptional regulation of Slit1 and Robo1 signaling.

To achieve the connectivity underlying normal brain function, axons grow along given pathways, taking directional decisions at specific points in space and time. These decisions depend on contacts of axons with guidance molecules and/or intermediate targets[1–3], which require axon growth to be tightly controlled. Axon growth rates may depend on both extracellular signals, such as those provided by neurotrophins and guidance molecules[4,5], and the identity and the state of maturation of the neuron, as illustrated by the loss of regrowth ability in the adult CNS[6,7].

Although it has long been known that neuronal activity is involved in the later stages of brain development, recent findings have suggested that spontaneous electrical activity before synapse formation can influence a wide range of developmental processes, from proliferation to transmitter specification and axon guidance[8,9]. Electrical stimulation of cultured embryonic neurons modulates axon extension in a cell-dependent manner[10–13]. Indeed, although electrical stimulation does not affect the growth rate of axons from spinal neurons[9], it strongly attenuates the growth of sensory axons[11,14]. Spontaneous electrical activity and its associated calcium transients have been shown to regulate the expression of specific subsets of genes that are important during development[15–17]. Thus, activity-dependent regulation of transcription may represent an important mechanism in the axonal growth program.

We tested this hypothesis by investigating whether spontaneous calcium activity serves as an intrinsic regulator of axon elongation in the thalamocortical system. The function of the neocortex is specifically governed by its innervation from the thalamus and virtually all sensory information passes through the thalamus *en route* to the cortex[18]. The distinct patterns that these axons display as they cross the telencephalon[19] suggest that thalamic neurons modulate the growth rate of their axons as they extend toward the cortex. We found that spontaneous Ca^{2+} activity and axonal growth rates were reduced when thalamocortical axons (TCAs) extended through the cortex. Ca^{2+} spikes modulated axonal growth through the transcriptional upregulation of the guidance receptor *Robo1*, which appeared to function as a brake for TCA growth. Thus, modifications in *Robo1* transcription that are triggered by spontaneous activity mediate the developmental decrease in axon growth.

RESULTS

The growth rate of TCAs is intrinsically regulated

TCAs travel a long distance through the forebrain before reaching their target cells in the neocortex[18]. DiI injection and calretinin immunostaining revealed that TCAs crossed the entire ventral telencephalon (vTel) in 2 d (embryonic days 12.5–14.5, E12.5–14.5), after which their rate of progress slowed as they passed through the cortical wall (E15.5–17.5; **Supplementary Fig. 1**). To analyze this switch, we measured the speed of growth of thalamocortical axons along distinct forebrain structures by two-photon time-lapse imaging in oblique thalamocortical slices after electroporation of *Gfp* into the thalamus (**Fig. 1a–c**). E13.5-electroporated thalamic axons at the vTel grew significantly faster than those axons extending through the cortex at E15.5 (E13.5, $63 \pm 2.6\ \mu m\ h^{-1}$, $n = 24$; E15.5, $38 \pm 2\ \mu m\ h^{-1}$, $n = 12$; $P < 0.001$; **Fig. 1d–l** and **Supplementary Videos 1** and **2**). Moreover, we followed

[1]Instituto de Neurociencias de Alicante, Universidad Miguel Hernández-Consejo Superior de Investigaciones Científicas (UMH-CSIC), San't Joan d'Alacant, Spain. [2]Ecole Normale Supérieure, Institut de Biologie de l'ENS, Paris, France. [3]INSERM, U1024, Avenir Team, Paris, France. [4]CNRS, UMR 8197, Paris, France. [5]Genentech, South San Francisco, California, USA. [6]The Rockefeller University, New York, New York, USA. [7]These authors contributed equally to this work. Correspondence should be addressed to G.L.-B. (g.lbendito@umh.es).

Received 3 May; accepted 8 June; published online 8 July 2012; doi:10.1038/nn.3160

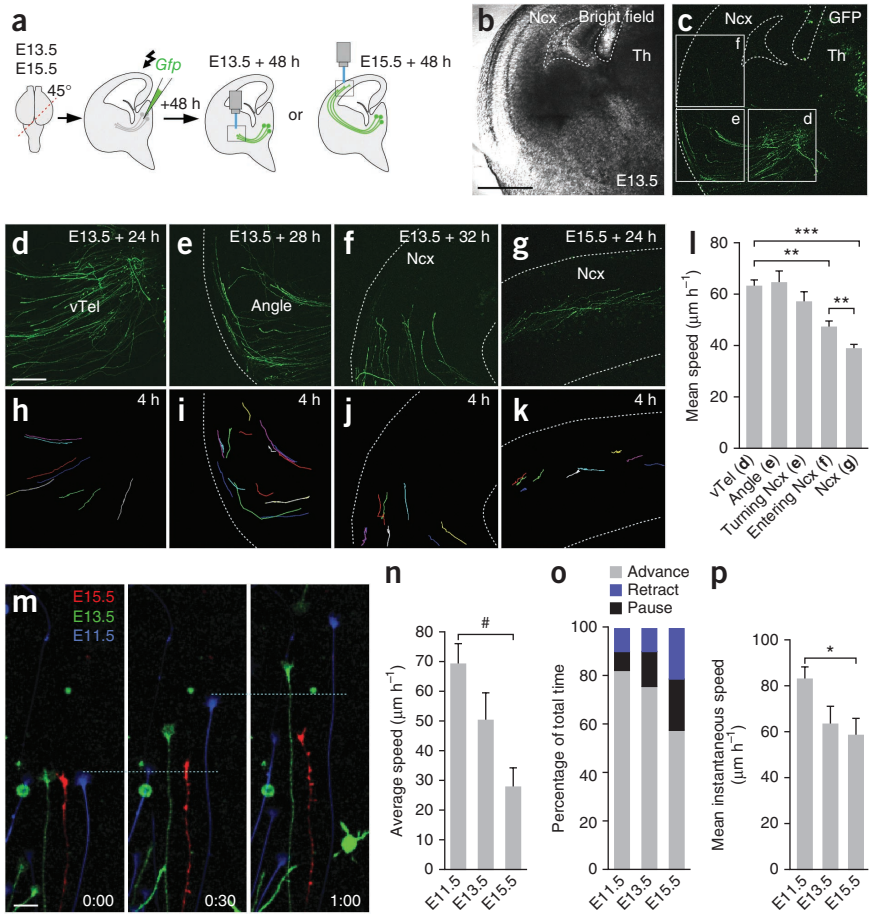

Figure 1 The speed of growth of TCAs is developmentally regulated. (**a**) Schematic representation of the experimental procedure used for time-lapse imaging of in-growing TCAs *ex vivo*. (**b**) Bright-field image showing an oblique thalamocortical slice use for the recordings. Ncx, neocortex; Th, thalamus. (**c**) *Gfp*-electroporated axons traversing several forebrain structures. (**d**–**g**) Examples of TCAs recorded at the level of the vTel (**d**), angle (**e**), entering the cortex (**f**) and extending through the neocortex (**g**) from E13.5 (**d**–**f**) and E15.5 (**g**) slices. (**h**–**k**) Track of axons in **d**–**g** measured after 4 h imaging. (**l**) Quantification of the data shown in **h**–**k**. $^{**}P < 0.01$, $^{***}P < 0.001$, one-way ANOVA test with Tukey's *post hoc* analysis. (**m**) Composite images of axons growing from E11.5 (blue), E13.5 (green) and E15.5 (red) thalamic explants from a 1-h time lapse showing axonal extension at 0, 30 and 60 min. For comparison, axonal growth cones were oriented in parallel and aligned at 0 min. Both E11.5 and E13.5 axons extended faster than E15.5. (**n**) The mean axon growth rate was calculated as the total extension over 1 h of the growth cone between the first and last frame. $^{\#}P < 0.01$, Kruskal-Wallis test with Dunn's *post hoc* analysis. (**o**) Proportion of the time spent by axons advancing, pausing or retracting at each stage studied. (**p**) The instantaneous velocity was defined as the average advancing velocity. $^{*}P < 0.05$, Kruskal-Wallis test with Dunn's *post hoc* analysis. The data are presented as mean ± s.e.m. Scale bars represent 500 μm (**b**,**c**), 200 μm (**d**–**g**) and 20 μm (**m**).

the same population of E13.5 axons when crossing several compartments and observed a steady decrease in axonal growth speed as axons approached the cortex (angle, 64 ± 4.7 μm h^{-1}, $n = 8$; turning, 57 ± 4.2 μm h^{-1}, $n = 9$; entering cortex, 47 ± 2 μm h^{-1}, $n = 10$; **Fig. 1d**–**l** and **Supplementary Videos 3** and **4**). Thus, an early phase of fast growth seems to be followed by a later phase of slow growth when TCAs extend across the neocortex. However, it remains unclear whether this switch in the rate of axon extension is controlled by environmental cues or by mechanisms intrinsic to the thalamus.

To determine whether thalamic neurons regulate their axon growth rate in accordance with their specific developmental stage, we transplanted thalamic tissue from a transgenic mice expressing GFP into the thalamus of wild-type host slices (**Supplementary Fig. 2**). Analysis of transplants of E13.5 GFP-expressing thalamic tissue (Th^{GFP}) into E13.5 or E15.5 host slices revealed that the majority of TCAs crossed the vTel and reached the cortex within 48 h (E13.5 to E13.5 mean score = 3.6 ± 0.32, $n = 19$; E13.5 to E15.5 mean score = 3.1 ± 0.4, $n = 9$; **Supplementary Fig. 2a**,**b**,**f**). However, when E15.5 Th^{GFP} were transplanted into E13.5 or E15.5 wild-type slices, TCAs extended slower and fewer axons reached the cortex (E15.5 to E13.5 mean score = 2 ± 0.32, $n = 19$; E15.5 to E15.5 mean score = 1.9 ± 0.34, $n = 13$; **Supplementary Fig. 2d**–**f**). Hence, the developmental state of thalamic neurons seems to influence the growth rate of their axons.

To further determine whether the axon growth rate is regulated by intrinsic factors in the thalamus, we examined the axonal speed of thalamic projecting neurons and the behavior of their growth cones on a poly-L-lysine/laminin substrate at different developmental stages (**Fig. 1m**–**p**). On average, axons from E11.5 and E13.5 explants grew notably faster than those of E15.5 thalamic explants (E11.5, 69 ± 6.7 μm h^{-1}, $n = 24$; E13.5, 50 ± 9 μm h^{-1}, $n = 19$; E15.5, 28 ± 6 μm h^{-1}, $n = 11$; **Fig. 1m**). As growing mammalian axons display saltatory behavior, we examined the interval of time that these axons spent advancing, pausing or retracting at each developmental stage. More mature thalamic axons experienced longer periods of retraction and longer pauses in their growth (**Fig. 1n**). Accordingly, TCAs advanced less at E15.5 than at earlier stages (58 ± 4.1% of total time at E15.5, 84 ± 3.2% at E11.5, 77 ± 4.8% at E13.5; **Fig. 1n**). When we measured the speed of growth of thalamic axons during the effective forward growth phase, a significant reduction was evident from E11.5 to E15.5 (E11.5, 83 ± 5.4 μm h^{-1}; E13.5, 63.4 ± 7.7 μm h^{-1}; E15.5, 58 ± 8.3 μm h^{-1}; $P < 0.001$; **Fig. 1p**). Hence, a developmental mechanism intrinsic to thalamic neurons appears to decrease the growth rate of TCAs as they approach the cortex.

Thalamic spontaneous activity is developmentally regulated

Neuronal activity is thought to influence neurite outgrowth by modulating intracellular calcium (Ca^{2+}) concentrations[20]. If spontaneous Ca^{2+} activity is responsible for the diminished axonal growth described above, features of this activity should change when the rate of axonal growth decreases. To characterize the developmental profile of spontaneous thalamic activity, we studied Ca^{2+} levels in the thalamus in oblique thalamocortical slices loaded with Oregon Green-BAPTA AM (**Fig. 2a**–**c**) or in which Oregon Green was injected at the level of the internal capsule to record Ca^{2+} spikes in thalamocortical projecting neurons (**Supplementary Fig. 3a**–**d**). Spontaneous

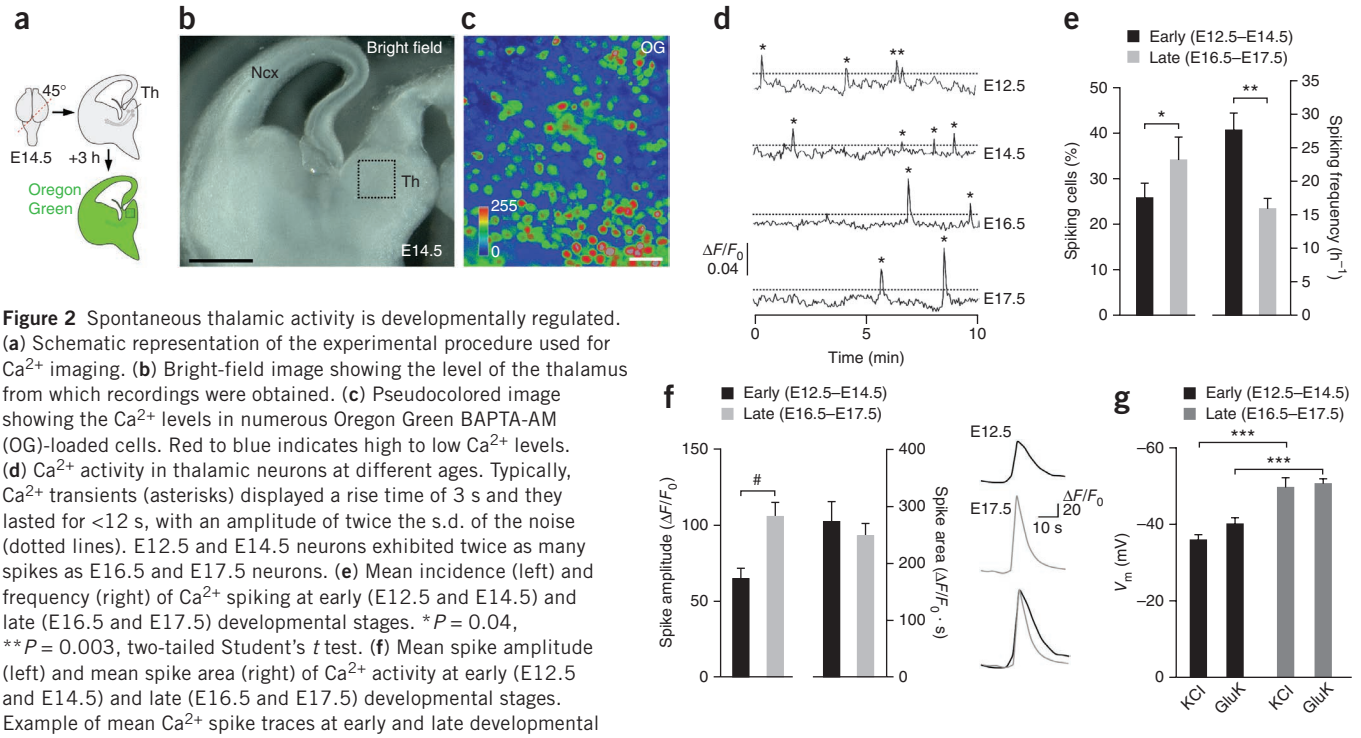

Figure 2 Spontaneous thalamic activity is developmentally regulated. (**a**) Schematic representation of the experimental procedure used for Ca^{2+} imaging. (**b**) Bright-field image showing the level of the thalamus from which recordings were obtained. (**c**) Pseudocolored image showing the Ca^{2+} levels in numerous Oregon Green BAPTA-AM (OG)-loaded cells. Red to blue indicates high to low Ca^{2+} levels. (**d**) Ca^{2+} activity in thalamic neurons at different ages. Typically, Ca^{2+} transients (asterisks) displayed a rise time of 3 s and they lasted for <12 s, with an amplitude of twice the s.d. of the noise (dotted lines). E12.5 and E14.5 neurons exhibited twice as many spikes as E16.5 and E17.5 neurons. (**e**) Mean incidence (left) and frequency (right) of Ca^{2+} spiking at early (E12.5 and E14.5) and late (E16.5 and E17.5) developmental stages. $^{*}P = 0.04$, $^{**}P = 0.003$, two-tailed Student's *t* test. (**f**) Mean spike amplitude (left) and mean spike area (right) of Ca^{2+} activity at early (E12.5 and E14.5) and late (E16.5 and E17.5) developmental stages. Example of mean Ca^{2+} spike traces at early and late developmental stages. $^{\#}P = 0.002$, two-tailed Student's *t* test. (**g**) Resting membrane potential recorded by whole-cell patch-clamp in thalamic neurons. GluK, potassium gluconate. $^{***}P < 0.001$, two-tailed Student's *t* test. Data are presented as mean ± s.e.m. Scale bars represent 300 µm (**b**) and 50 µm (**c**).

Ca^{2+} transients were identified in thalamic neurons at all embryonic stages studied and we were able to distinguish two phases in the developmental pattern of this activity, which correlated with those observed for axon growth. During the early phase (E12.5–14.5), spontaneous Ca^{2+} spikes occurred in thalamic neurons with an incidence of 25.8 ± 3.4% and a frequency of 27.9 ± 2.6 h^{-1}, as determined in 10-min recording periods (311 cells pooled from $n = 12$ E12.5–14.5 slices; **Fig. 2d**,**e** and **Supplementary Video 5**). However, during the late phase (E16.5–17.5) 34.3 ± 5.1% of cells develop Ca^{2+} spikes with a frequency of 16.2 ± 1.5 h^{-1} (385 cells pooled from $n = 9$ E16.5–17.5 slices; **Fig. 2d**,**e** and **Supplementary Video 6**), indicating that, although the proportion of cells with Ca^{2+} transients increased, the frequency diminished during embryonic development. This developmental decrease in spontaneous Ca^{2+} activity in thalamic neurons also occurred at the growth cones (**Supplementary Fig. 3e–g** and **Supplementary Videos 7** and **8**). Moreover, the amplitude of the somatic Ca^{2+} transients increased as development proceeded (early, 65.0 ± 6.5 $\Delta F/F_0$, $n = 29$ cells; late, 105.9 ± 8.8 $\Delta F/F_0$, $n = 51$ cells; **Fig. 2f**), yet their spike area did not change between the distinct developmental stages assayed (early, 274.5 ± 35 $\Delta F/F_0 \cdot s$, $n = 29$ cells; late, 248.6 ± 21 $\Delta F/F_0 \cdot s$, $n = 51$ cells; **Fig. 2f**). Thus, the reduced spike frequency at later developmental stages suggests that the number of elevations of intracellular Ca^{2+} that a given cell experiences per unit time decreases.

The reduction in the firing probability observed at later stages was correlated with a change in the resting membrane potential (V_m). Indeed, late phase thalamic neurons were more hyperpolarized than at earlier stages, as measured with both KCl and potassium gluconate internal solution (KCl, −35.8 ± 1.2 mV at early stages, $n = 33$ cells; −49.5 ± 3 mV at later stages, $n = 16$ cells; potassium gluconate, −40 ± 1.6 mV at early stages, $n = 24$ cells; −50.8 ± 1.1 mV at later stages, $n = 21$ cells; **Fig. 2g**), indicating that voltage-operated channels may contribute to spontaneous thalamic activity. Together, these results indicate that both spontaneous thalamic activity and resting V_m are developmentally regulated, following a biphasic profile reminiscent of that observed for axon growth.

Silencing spontaneous activity slows TCA growth

The correlation observed above suggests that the profile of spontaneous activity in the thalamus may serve as an intrinsic regulator of axon growth, with high Ca^{2+} frequencies inducing faster growth at earlier stages and lower frequencies attenuating axon extension later on. We tested this hypothesis by blocking L-type voltage-operated Ca^{2+} channels (VOCCs) with 10 µM of nifedipine, as other VOCCs types do not contribute as much to this activity (**Supplementary Fig. 4a**). Nifedipine reduced the frequency of spontaneous Ca^{2+} spikes in early-stage neurons, producing a profile resembling that of more mature neurons (control, 27.9 ± 1.3 h^{-1}, $n = 314$ cells; nifedipine, 16.8 ± 2.0 h^{-1}, $n = 45$ cells; **Fig. 3a**). As the profile of Ca^{2+} transients was preserved in thalamic explants grown on poly-L-lysine/laminin (**Supplementary Fig. 4b–f**), we expected that decreasing the spontaneous Ca^{2+} frequency through L-type VOCC blockade would decrease axonal extension in early thalamic neurons. Indeed, the axons in E13.5 thalamic explants cultured for 48 h in the presence of nifedipine were shorter than those grown under control conditions (control, 100 ± 8.4%, $n = 30$; nifedipine, 58.4 ± 4.4%, $n = 28$; **Fig. 3b–d**). Conversely, axons of early thalamic neurons grew longer when their activity was increased by elevating the KCl concentration in the extracellular medium (5 mM control, 100 ± 9%, $n = 44$; 7.5–10 mM, 132.4 ± 5.1%, $n = 83$; 12.5–15 mM, 120.7 ± 6.7%, $n = 70$; **Fig. 3a**,**e–g**). Although elevated KCl depolarized late thalamic neurons, it did not increase their axonal outgrowth (**Supplementary Fig. 4g–j**). Moreover, addition of nifedipine had no effect in the Ca^{2+} frequency of these neurons (**Supplementary Fig. 4k**). Thus, it appears that the specific developmental profiles of spontaneous thalamic activity define the rate of axon extension, at least *in vitro*.

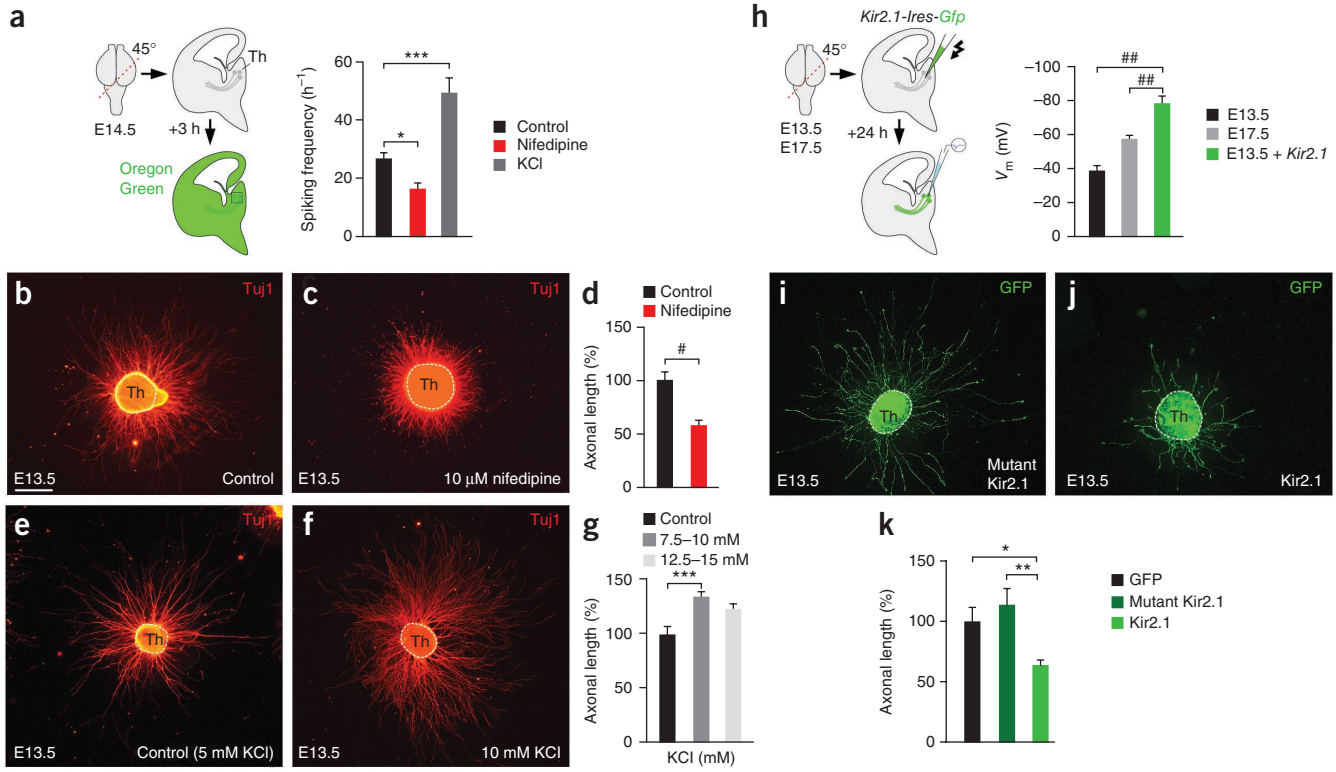

Figure 3 Manipulation of spontaneous thalamic activity alters the axon growth rate. (**a**) Experimental procedure used for Ca^{2+} imaging in the presence of 10 μM nifedipine or 10 mM KCl. Blocking L-type VOCCs with nifedipine decreased spontaneous Ca^{2+} activity to levels similar to those seen at later stages. KCl increased the frequency of Ca^{2+} activity in E14.5 neurons (49.5 ± 5.3 h^{-1}, $n = 53$ cells). $^{*}P < 0.05$, $^{***}P < 0.001$, Kruskal-Wallis test with Dunn's *post hoc* analysis. (**b**,**c**) Tuj1 revealed that blocking L-type VOCC with 10 μM nifedipine decreased TCA length. (**d**) Quantification of the data shown in **b** and **c** (control, 173 ± 15 μm; nifedipine, 101 ± 7 μm). $^{\#}P < 0.001$, Mann-Whitney *U*-test. (**e**,**f**) Tuj1 revealed increased TCA growth following chronic depolarization. (**g**) Quantification of the data shown in **e** and **f**. When $[KCl]_o$ was elevated to 7.5–10 mM, axon growth increased significantly when compared with control conditions (control, 116 ± 10 μm; 7.5–10 mM, 154 ± 6 μm; 12.5–15 mM, 141 ± 8 μm). (**h**) Experimental procedure used to assess the effect of *Kir2.1* on the resting membrane potential at two developmental stages (E13.5 and E17.5). $^{\#\#}P < 0.001$, two-tailed Student's *t* test. (**i**,**j**) GFP immunostaining revealed a decrease in axon length after forced hyperpolarization. (**k**) Quantification of the data shown in **i** and **j** and data not shown. $^{**}P < 0.01$, Kruskal-Wallis test with Dunn's *post hoc* analysis. Data are presented as mean ± s.e.m. Scale bar represents 300 μm.

The changes in membrane potential that occur during embryonic development may also affect TCA growth. To assess these effects, we overexpressed the human inwardly rectifying potassium channel Kir2.1 in thalamic neurons, which causes hyperpolarization and a substantial decrease in neural activity both *in vitro* and *in vivo*[21–23]. As expected, Kir2.1 overexpression shifted the resting membrane potential in thalamic neurons from −39.2 ± 2.4 mV to −79 ± 4.0 mV at E13.5, and from −57.6 ± 2.3 mV to −77 ± 0.9 mV at E17.5 (E13.5, $n = 3$–9; E17.5, $n = 6$–9; **Fig. 3h** and data not shown). Kir2.1 overexpression in E13.5 thalamic explants markedly reduced TCA growth when compared with overexpression of a nonconductive form of this channel (mutant Kir2.1), which did not significantly affect thalamic axon length (GFP, 100 ± 12.4%, $n = 20$; mutant Kir2.1, 112 ± 14.5%, $n = 14$; Kir2.1, 63.7 ± 4%, $n = 24$; $P > 0.05$; **Fig. 3i**,**k**). Together, these findings indicate that modifications to the profile of spontaneous activity or alterations to the resting membrane potential are both sufficient to modulate the rate of TCA growth during development.

If the frequency of intracellular Ca^{2+} transients influences the TCA growth rate, blocking these transients at early stages might be sufficient to prematurely attenuate TCA extension *in vivo*. We assessed this possibility in early thalamic neurons that were hyperpolarized following targeted *in utero* electroporation of *Kcnj2* (the gene encoding Kir2.1) at E12.5. Spontaneous Ca^{2+} transients were markedly reduced by Kir2.1 overexpression in both soma and growth cones (**Supplementary Fig. 5**), confirming that spontaneous activity depends on the resting membrane potential. The thalamus was co-electroporated with plasmids encoding Kir2.1 or mutant Kir2.1 and a plasmid bearing *Gfp* to assess the cortical extension of GFP-labeled axons at E15.5 (**Fig. 4a**–**d**). Hoechst staining revealed no difference in cell death in brains electroporated with *Kir2.1* or mutant *Kir2.1* (data not shown). At this stage, primarily rostral and intermediate levels of the thalamus are targeted by electroporation and TCAs could be visualized and quantified at rostral and intermediate levels of the neocortex (**Fig. 4b**,**c** and **Supplementary Fig. 6**). TCAs electroporated with mutant *Kir2.1* traversed long distances and crossed more than half of the developing neocortex at both levels (mutant *Kir2.1*, 0.77 ± 0.02, $n = 11$; **Fig. 4**). In contrast, we observed a significant delay in TCA progression in *Kir2.1*-electroporated brains at both rostral and intermediate cortical levels (*Kir2.1*, 0.62 ± 0.03, $n = 10$; $P < 0.001$; **Fig. 4g**–**i**). Moreover, GFP fluorescence in *Kir2.1*-electroporated brains was more intense in the lateral part of the neocortex, suggesting that many silenced TCAs accumulated in the neocortex at this stage. These findings suggest that silencing spontaneous thalamic activity attenuates TCA extension *in vivo*, consistent with our *in vitro* results.

Silencing spontaneous activity augments the levels of *Robo1*

Both the frequency and pattern of electrical activity regulate the expression of subsets of genes involved in neuronal development[16,24,25]. We investigated whether spontaneous thalamic activity modulates

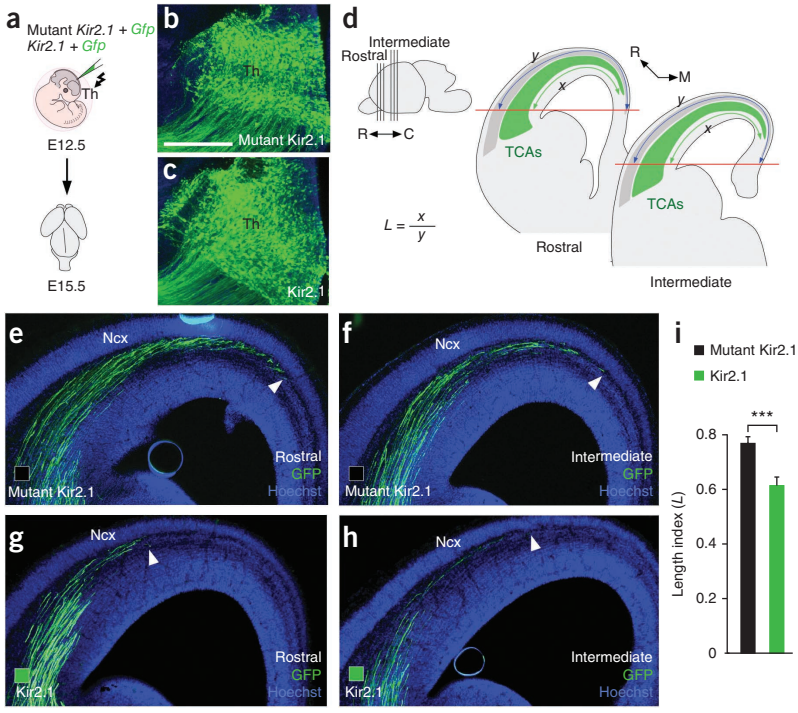

Figure 4 Silencing spontaneous thalamic activity attenuates TCA elongation *in vivo*. (**a**) Schematic representation of the experimental procedure used to test the effect of silencing thalamic activity *in vivo*. The mutant *Kir2.1* or *Kir2.1* plasmids were co-electroporated with *Gfp* into the thalamus *in utero* at E12.5 and the brains were analyzed at E15.5, at the peak of TCA cortical extension. (**b**,**c**) GFP expression in the thalamus reflecting the extent of electroporation in both conditions. (**d**) Schematic representation of the method to quantify and calculate the cortical extension along the rostro-caudal axis of the cerebral wall. The maximum distance reached by GFP-positive axons (*x*, green line) was measured at two rostro-caudal levels from a horizontal line passing tangential to the ventricular edge of the pallial-subpallial boundary (red line) and normalized to the total length (*y*, blue line) of the cortical area defined by the lateral and medial intersections of this line in the cortical wall. (**e**–**h**) Coronal sections from rostral (**e**,**g**) and intermediate (**f**,**h**) levels of electroporated brains revealed the delay in cortical invasion by GFP-positive axons (arrowheads) in *Kir2.1* and mutant *Kir2.1* electroporated neurons. (**i**) Quantification of the data shown in **e**–**h**. ***$P < 0.001$, two-tailed Student's *t* test. The data are presented as mean ± s.e.m. Scale bar represents 300 μm and applies to all panels.

TCA growth by regulating the expression of genes involved in the development of thalamocortical connectivity. Thalamic explants were electroporated with plasmids expressing GFP and either Kir2.1 or mutant Kir2.1, and were analyzed after 72 h in culture. Among the genes studied, we identified *Robo1* as a major target of thalamic spontaneous activity. Semi-quantitative reverse transcription (RT)-PCR using two sets of primers revealed a marked increase in the expression of the *Robo1*, but not the *Robo2*, gene in thalamic neurons expressing

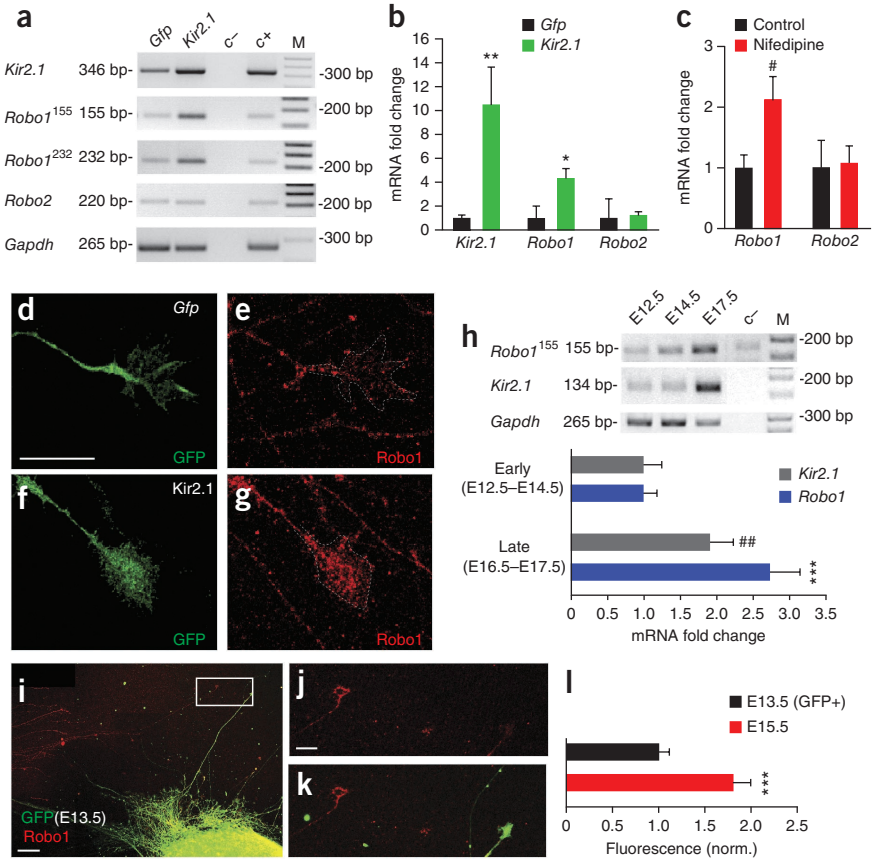

Figure 5 Silencing thalamic activity upregulates Robo1 transcription. (**a**) Semi-quantitative PCR comparing transcript levels in active and silenced thalamic cells using primers for *Gapdh* (control), *Kir2.1*, *Robo2* and two sets of primers for *Robo1* (generating 155-bp and 232-bp products). Total thalamic cDNA was used as a positive control (c+). M, molecular marker. c–, negative control. (**b**) Real-time PCR quantification of the transcripts for *Kir2.1*, *Robo1* and *Robo2* in *Gfp* and *Kir2.1*-electroporated cells. *$P = 0.03$, **$P = 0.003$, two-tailed Student's *t* test. (**c**) Real-time PCR quantification of the transcripts for *Robo1* and *Robo2* after decreasing spontaneous Ca^{2+} activity by nifedipine treatment. #$P = 0.006$, two-tailed Student's *t* test. (**d**–**g**) Immunohistochemistry for Robo1 in control (**d**,**e**) and Kir2.1-expressing axons (**f**,**g**). (**h**) Semiquantitative PCR for *Kir2.1*, *Robo1* and *Gapdh*. Expression of *Kir2.1* and *Robo1* were normalized to that of *Gapdh* and to the E12.5 value. Full-length gels are presented in **Supplementary Figure 9**. ##$P = 0.02$, ***$P < 0.001$, two-tailed Student's *t* test. (**i**–**k**) Immunohistochemistry for Robo1 in E13.5 (GFP-positive) and E15.5 isolated thalamic growth cones. Thalamic explants from E13.5 GFP-expressing mice were co-cultured together with explants from wild-type E15.5 embryos on poly-L-lysine/laminin coverslips. (**l**) Quantification of the data shown in **j**. ***$P < 0.001$, two-tailed Student's *t* test. The data are presented as mean ± s.e.m. Scale bars represent 15 μm (**d**–**g**), 50 μm (**i**) and 15 μm (**j**,**k**).

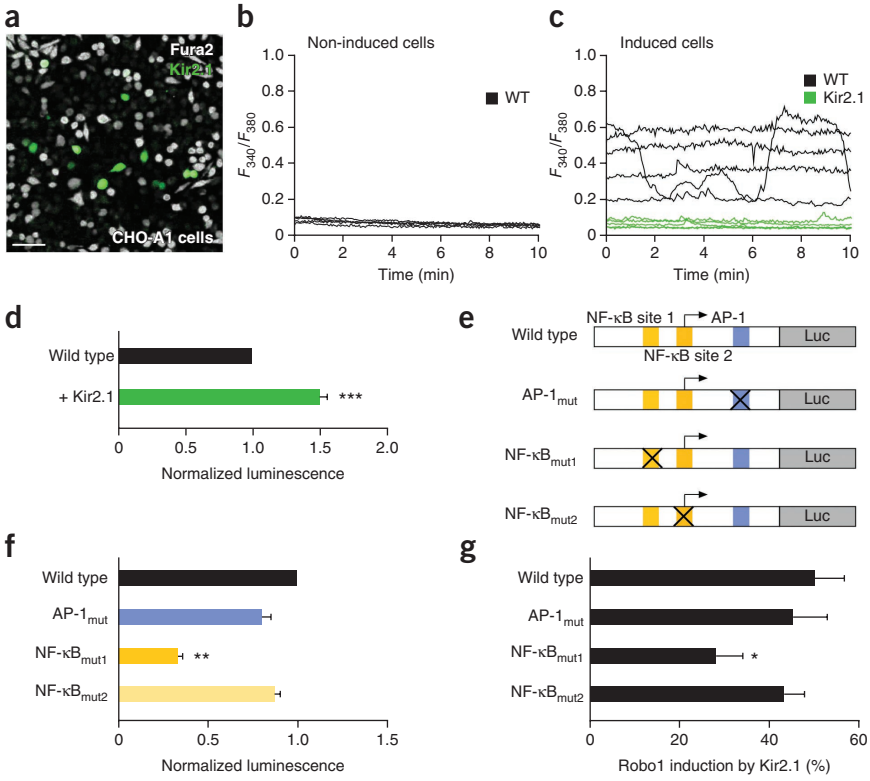

Figure 6 Robo1 expression is regulated at the transcriptional level through a NF-κB binding site. (**a**–**c**) CHO-A1 cells transfected with the *Kir2.1* construct and loaded with Fura2 calcium indicator. Following tetracycline administration, TRPA1 channels were upregulated and a strong spontaneous Ca^{2+} activity was generated (black traces in **b** and **c**), which could be blocked by *Kir2.1* electroporation (green traces). WT, wild type. (**d**) Silencing spontaneous activity induced a 1.5-fold increase in expression of the luciferase reporter. $^{***}P < 0.001$, two-tailed Student's *t* test. (**e**) Schematic representations of the wild-type and mutated forms of the 2,446-bp cloned region of the *Robo1* promoter. (**f**) There was strong reduction in the basal transcription of *Robo1* when the NF-κB site 1 was mutated, but no significant reduction when the AP-1 or the NF-κB sites 2 were mutated ($n \geq 3$ replicates). $^{**}P < 0.001$, Kruskal-Wallis test with Dunn's *post hoc* analysis. (**g**) Luciferase assays to evaluate the contribution of AP-1 and NF-κB sites to the Robo1 induction by *Kir2.1*. Only mutating the NF-κB site 1 significantly reduced the induction of *Robo1* transcription after silencing spontaneous activity ($n \geq 3$ replicates). $^{*}P < 0.05$, Mann-Whitney *U*-test. Data are presented as mean ± s.e.m. Scale bar represents 50 μm.

Kir2.1 (**Fig. 5a**). When assessed by quantitative RT-PCR, silencing thalamic neuronal activity increased the expression of *Robo1* 4.3-fold in Kir2.1-expressing thalamic neurons (GFP, $n = 6$; Kir2.1, $n = 7$; **Fig. 5b**), whereas *Robo2* expression did not differ significantly from that in controls ($P > 0.05$; **Fig. 5b**). The presence of nifedipine, which mimics the developmental reduction of spontaneous Ca^{2+} spikes, produced a 2.1-fold increase in *Robo1* transcripts (control, $n = 10$; nifedipine, $n = 10$; **Fig. 5c**), without affecting the expression of *Robo2* (control, 1.0 ± 0.4, $n = 10$; nifedipine, 1.07 ± 0.3 $n = 9$; **Fig. 5c**). Robo1 protein levels were accordingly increased in *Kir2.1*-electroporated axons (**Fig. 5d**–**g**).

Robo1 transcript levels *in vivo* increased naturally in the thalamus throughout embryonic development (1.00 ± 0.20 at early stages, $n = 14$; 2.73 ± 0.41 at late stages, $n = 13$; **Fig. 5h**), as did the Robo1 protein detected in isolated thalamic growth cones (1.00 ± 0.11 at early stages, $n = 25$; 1.81 ± 0.18 at late stages $n = 25$; **Fig. 5i**–**l**). Thus, the upregulation of the Robo1 receptor could contribute to the change in growth rate that we observed in these neurons. Endogenous *Kir2.1* expression was stronger at later rather than at early stages of thalamic development (1.00 ± 0.26 at early stages, $n = 5$; 1.91 ± 0.33 at late stages, $n = 4$; **Fig. 5h**). Together, these results indicate that developmental changes in spontaneous thalamic activity regulate the expression of the guidance receptor Robo1.

A NF-κB binding site mediates *Robo1* transcriptional regulation

To determine whether the change in Robo1 expression induced by spontaneous activity occurs at the transcriptional level, we first searched for conserved motifs associated with Ca^{2+}-sensitive transcription factors in the regulatory sequences of the *Robo1* gene. Sequence alignment revealed a 2,446-bp evolutionarily conserved region upstream of the first exon (**Supplementary Fig. 7a**), which we cloned upstream of the firefly *luciferase* gene. We transfected this Robo1 reporter into inducible Chinese hamster ovary (CHO)-A1 cells that express TRPA1 channels following tetracycline administration[26]. After induction, strong spontaneous Ca^{2+} activity is generated in these cells that can be silenced by *Kir2.1* transfection (**Fig. 6a**–**c**). Silencing spontaneous activity induced a 1.5-fold increase in Robo1 reporter activity in these cells (*Kir2.1*, 1.5 ± 0.06, $n = 11$ experiments; **Fig. 6d**), but not in cells with no spontaneous activity (**Supplementary Fig. 7c**–**e**). Thus, Ca^{2+} elevations regulate the transcription of *Robo1*, indicating that there may be activity-responsive elements in the *Robo1* promoter. Only one activator protein 1 (AP-1) site and two NF-κB transcription factor binding sites (sites 1 and 2; **Fig. 6e**) were particularly conserved in terms of sequence and position among the mammalian genomes analyzed, suggesting that these sites might be important for the regulation of *Robo1* transcription (**Supplementary Fig. 7**). Both transcription factors have been implicated in activity-dependent transcriptional regulation[27,28]. Mutating NF-κB site 1 in the Robo1 reporter induced a strong reduction in the basal transcription of *Robo1* (wild type: 1, $n = 11$; NF-κB site 1: 0.33 ± 0.03, $n = 12$; **Fig. 6f**) that was not observed when the AP-1 site or NF-κB site 2 were mutated (AP-1: 0.79 ± 0.05, $n = 11$; NF-κB site 2: 0.86 ± 0.03, $n = 7$; **Fig. 6f**). These results indicate that NF-κB site 1 is essential for *Robo1* transcription.

To determine whether the *Robo1* regulation by activity was dependent on these sites, we tested how their mutation would affect the Kir2.1-induced increase in *Robo1* promoter activity (**Fig. 6e**). Neither mutations in NF-κB site 2 nor AP-1 affected the fractional increase of *Robo1* transcription by Kir2.1 (wild type + Kir2.1, 49.5 ± 6.0%, $n = 11$ experiments; mutant AP-1 + Kir2.1, 46 ± 6.6%, $n = 8$; mutant NF-κB site 2 + Kir2.1, 39.5 ± 5.0%, $n = 6$; **Fig. 6g**). Mutating the NF-κB site 1 dampened the effect produced by Kir2.1 overexpression by 43% (mutant NF-κB site 1 + Kir2.1, 28.4 ± 5.0%, $n = 7$; **Fig. 6g**). Thus, NF-κB site 1 appears to be important for both basal and activity-dependent transcription of *Robo1*.

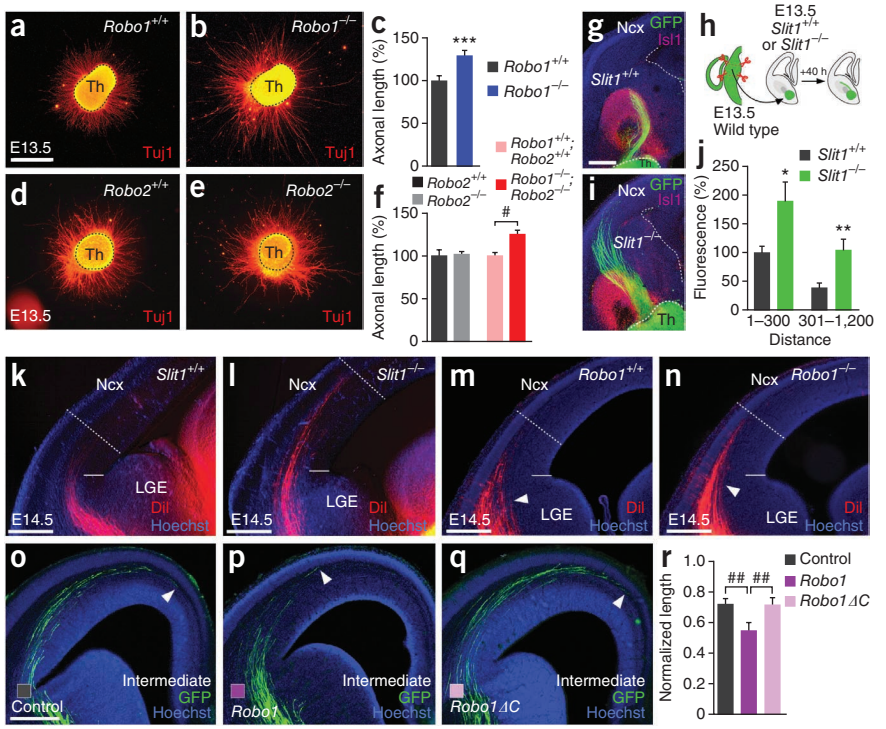

Figure 7 Loss of *Robo1* increases the intrinsic capacity for thalamic outgrowth. (**a**,**b**) Tuj1 immunostaining revealed that thalamic axon growth increased in the absence of Robo1. (**c**) Quantification of the data shown in **a** and **b**. ***$P < 0.001$, Student's *t* test. (**d**,**e**) Tuj1 immunostaining revealed that the absence of the *Robo2* receptor did not affect thalamic axon growth *in vitro*. (**f**) Quantification of the data shown in **d** and **e**, and data not shown. #$P < 0.001$, two-tailed Student's *t* test. (**g**,**i**) Wild-type thalamic axons from a GFP-expressing mouse grew significantly more in *Slit1*$^{-/-}$ slices than in control slices. Islet1 labeled the corridor at the subpallial region. (**h**) Experimental procedure used to analyze the involvement of Slit1 in thalamic growth. (**j**) Quantification of the data shown in **g** and **i**. Normalized fluorescence was measured from the border of the explant. *$P = 0.03$ and **$P = 0.007$, two-tailed Student's *t* test. (**k**,**l**) Progression of TCAs labeled by DiI in the E14.5 thalamus of *Slit1*$^{+/+}$ and *Slit1*$^{-/-}$ brains. (**m**,**n**) Progression of TCAs labeled by DiI in the E14.5 thalamus in *Robo1*$^{+/+}$ and *Robo1*$^{-/-}$ brains. (**o**–**q**) GFP-immunoreactive axons in coronal sections at intermediate cortical levels. Overexpression of Robo1 (**p**) led to a significant delay in the cortical extension of TCAs when compared with controls. Electroporation of a truncated *Robo1* lacking the CC2 and CC3 domains (**q**) failed to significantly alter TCA cortical extension when compared with controls. (**r**) Quantification of the data shown in **o**–**q**. ##$P < 0.05$, one-way ANOVA test with Tukey's *post hoc* analysis. Data are presented as mean ± s.e.m. Scale bars represent 300 μm.

Robo1 functions as an intrinsic brake for TCAs

To assess whether Robo1 regulates TCA growth during development, we quantified axonal outgrowth in thalamic explants from wild-type and *Robo1*-deficient mice (**Fig. 7**). We found that axons grew more in the absence of *Robo1* (*Robo1*$^{+/+}$, 100 ± 4.6%, $n = 22$; *Robo1*$^{-/-}$, 132.8 ± 6.3%, $n = 24$; **Fig. 7a–c**). We tested whether this effect was specific to Robo1 by performing similar experiments using *Robo2*$^{-/-}$ and *Robo1*$^{-/-}$; *Robo2*$^{-/-}$ double mutant mice. There was no difference in thalamic axonal outgrowth in the absence of *Robo2* (*Robo2*$^{+/+}$, 100 ± 6.3%, $n = 29$; *Robo2*$^{-/-}$, 101.1 ± 3.0%, $n = 32$; **Fig. 7d–f**), whereas the loss of both genes produced a similar increase in length as the absence of *Robo1* alone (*Robo1*$^{+/+}$; *Robo2*$^{+/+}$, 100 ± 3.6%, $n = 82$; *Robo1*$^{-/-}$; *Robo2*$^{-/-}$, 125 ± 4.2%, $n = 105$; **Fig. 7f** and data not shown). In conjunction with our quantitative PCR (qPCR) data showing Robo1 specificity, these results indicate that Robo1, but not Robo2, acts as an intrinsic brake for thalamic axon progression.

As Robo proteins are best known as receptors for the secreted Slit guidance cues, we wondered whether Slits were involved in the modulation of TCA growth. Although Slit2 is mainly expressed in the proliferative zone of the thalamus, Slit1 is distributed along the entire pathway of TCA connectivity[29]. Thalamic explants from GFP-expressing embryos were placed into telencephalic slices from *Slit1*$^{-/-}$ mutant mice or wild-type littermates. TCAs extended significantly further when grown in *Slit1*$^{-/-}$ slices than in controls (*Slit1*$^{+/+}$, 100 ± 10.7% (0–300), 37.6 ± 8.8% (301–1,200), $n = 8$ explants; *Slit1*$^{-/-}$, 189.4 ± 32.7% (0–300), 105.1 ± 18.2% (301–1,200), $n = 6$ explants; $P < 0.03$; **Fig. 7g–j**), indicating that Slit1 slows down TCA progression in the telencephalon.

Slit1 and Robo1 signaling regulates TCA growth *in vivo*

It appears that Slit1 and Robo1 signaling influences thalamic axonal extension both *in vitro* and *ex vivo*. We tested whether this effect also occurs *in vivo* by performing anterograde DiI tracing in *Slit1*$^{-/-}$ and *Robo1*$^{-/-}$ mutant mice at E14.5. The lack of either *Slit1* or *Robo1* accelerated TCA extension in the neocortex when compared with that seen in wild-type mice (*Slit1*$^{+/+}$, $n = 4$; *Slit1*$^{-/-}$, $n = 4$; *Robo1*$^{+/+}$, $n = 3$; *Robo1*$^{-/-}$, $n = 5$; **Fig. 7k–n**).

We predicted that increasing Robo1 levels in thalamic neurons would attenuate TCA growth, mimicking the effects of *Kir2.1*-induced silencing of thalamic spontaneous activity. We augmented Robo1 levels through targeted *in utero* electroporation in thalamic neurons of a full-length Robo1 at E12.5 and we quantified the extension of TCAs. The exogenous expression of Robo1, but not GFP, notably diminished TCA extension (GFP, 0.73 ± 0.03, $n = 8$; full-length *Robo1*, 0.55 ± 0.05, $n = 9$; **Fig. 7o,p,r**), and TCAs stalled at the lateral regions of the cortical wall, in some cases barely crossing the pallial subpallial boundary (data not shown). Together, these results indicate that Robo1 gain-of-function mimics the effects observed when thalamic spontaneous activity is silenced, supporting the proposed role of Robo1 as a brake for TCA extension.

To determine whether Robo1 signaling is necessary to attenuate thalamic axonal growth, we used a truncated form of Robo1 (Robo1ΔC) that lacks the CC2 and CC3 intracellular domains required to transduce Slit signals to the cytoskeleton[30]. As expected, Robo1ΔC expression in thalamic neurons decreased Slit-dependent growth cone collapse (data not shown) and, in contrast with *Robo1*, electroporation of *Robo1*ΔC did not attenuate cortical extension of thalamic axons *in vivo* when compared with control brains (*Robo1*ΔC, 0.72 ± 0.04, $n = 9$. **Fig. 7q,r**). Thus, the CC2 and CC3 intracellular domains appear to be required for Robo1 to attenuate axon growth.

Robo1 functions downstream of spontaneous activity

Both overexpression of Robo1 and the silencing of spontaneous activity in the embryonic thalamus delay TCA progression. We hypothesized that the increase in Robo1 signaling in electrically silent

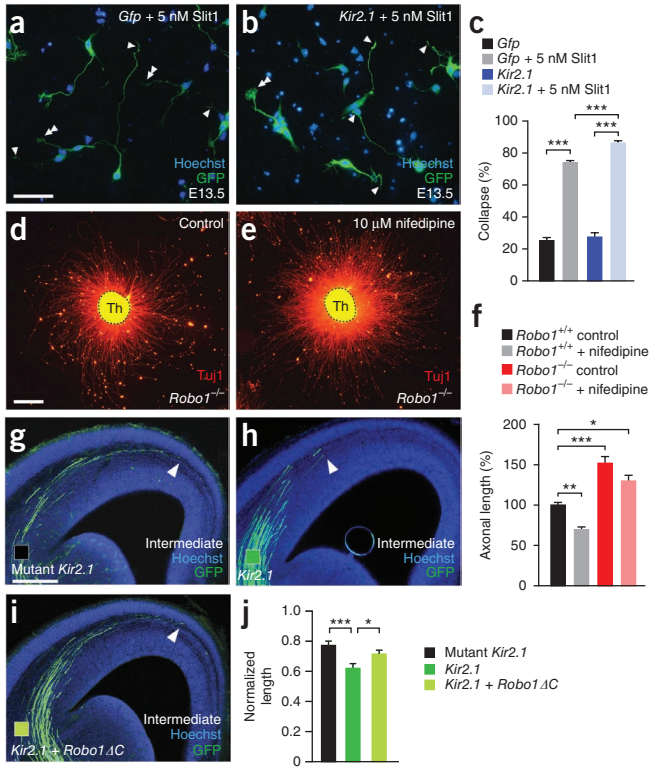

Figure 8 Robo1 controls axon extension *in vivo* downstream of spontaneous activity. (**a**,**b**) GFP (green) and Hoechst (blue) staining in control (*Gfp*, **a**) and *Kir2.1*-tranfected (**b**) dissociated thalamic cells after treatment with 5 nM Slit1. Addition of recombinant Slit1 significantly increased thalamic growth cone collapse in *Kir2.1*-transfected cells compared with controls. (**c**) Quantification of the data shown in **a** and **b**. $^{***}P < 0.001$, one-way ANOVA test with Tukey's *post hoc* analysis. (**d**,**e**) Tuj1 staining in E13.5 *Robo1*$^{-/-}$ thalamic explants after treatment with 10 μM nifedipine. Addition of nifedipine did not significantly change the increased thalamic growth observed in the Robo1 mutants. (**f**) Quantification of the data shown in **d** and **e** (*Robo1*$^{+/+}$ control, 288 ± 9.8 μm; *Robo1*$^{+/+}$ + nifedipine, 201 ± 8.8 μm; *Robo1*$^{-/-}$ control, 437 ± 24 μm; *Robo1*$^{-/-}$ + nifedipine, 372 ± 21 μm). $^{*}P < 0.05$, $^{**}P < 0.01$, $^{***}P < 0.001$, one-way ANOVA test with Tukey's *post hoc* analysis. (**g**–**i**) Coronal sections showing GFP-labeled axons at intermediate cortical levels following electroporation with mutant *Kir2.1*, *Kir2.1* and *Kir2.1* + *Robo1ΔC*. Co-electroporation of *Robo1ΔC* with *Kir2.1* rescued the defective cortical progression of TCAs following electroporation with *Kir2.1* alone. (**j**) Quantification of the data shown in **g**–**i**. $^{*}P < 0.05$, $^{***}P < 0.001$, one-way ANOVA test with Tukey's *post hoc* analysis. Data are presented as mean ± s.e.m. Scale bars represent 50 μm (**a**,**b**) and 300 μm (**d**,**e** and **g**–**i**).

neurons is an important step for producing a deceleration in axon growth. Addition of 5 nM of Slit1 to dissociated thalamic cultures significantly augmented growth cone collapse of Kir2.1-expressing axons compared with those transfected with *Gfp* (Kir2.1, 86 ± 1%, n = 1,112 growth cones from five independent experiments; *Gfp*, 73 ± 0.7%, n = 1,107 growth cones from five independent experiments; $P < 0.001$; **Fig. 8a**–**c**), suggesting an increase of Slit-Robo1 signaling in silenced axons. Moreover, addition of 10 μM nifedipine to *Robo1*$^{-/-}$ thalamic explants did not significantly reduce the increased growth observed in these mice (*Robo1*$^{+/+}$, 100 ± 3.4%, n = 26; *Robo1*$^{+/+}$ + nifedipine, 70 ± 3%, n = 29; *Robo1*$^{-/-}$, 152 ± 8.5%, n = 32 from five different knockouts; *Robo1*$^{-/-}$ + nifedipine, 129 ± 7.2%, n = 27; $P < 0.05$; **Fig. 8d**–**f**), indicating that the reduction of axon growth induced by blocking L-type VOCCs occurs through Robo1 receptors.

To determine the extent to which spontaneous thalamic activity influences TCA growth rate via Robo1 *in vivo*, we quantified axon growth in thalamic neurons co-electroporated with *Kir2.1* and *Robo1ΔC* at E12.5. In contrast with the deficient axon progression seen following *Kir2.1* electroporation alone, TCA extension following co-electroporation with *Kir2.1* and *Robo1ΔC* did not differ significantly from that in controls ($P > 0.05$), except for 3 cases out of 16 brains in which the delay was largely persistent. Accordingly, in the remaining cases, TCAs from neurons co-electroporated with plasmids expressing *Kir2.1* and *Robo1ΔC* extended significantly further into the cortex than those expressing *Kir2.1* alone (*Kir2.1*, 0.62 ± 0.03, n = 10; *Robo1ΔC* + *Kir2.1*, 0.72 ± 0.02, n = 13; mutant *Kir2.1*, 0.77 ± 0.02, n = 11; $P < 0.05$; **Fig. 8g**–**j**). These results indicate that interfering with Robo1 function can rescue the attenuated axon growth provoked by the silencing of spontaneous thalamic activity *in vivo*.

DISCUSSION

Regulating axonal growth is thought to be critical to correctly wire the brain, yet we still know little about the mechanisms that temporally control the extension of axons. Using the thalamocortical system as a model, we identified spontaneous activity as an intrinsic modulator of the extension rate of developing axons. We found that a developmental switch in TCA growth rate occurred concurrently with a decrease in spontaneous Ca^{2+} activity. This decrease in Ca^{2+} activity was sufficient to control the slowing down of axonal extension during cortical progression of TCAs (**Supplementary Fig. 8**). Spontaneous thalamic Ca^{2+} activity controlled TCA growth by regulating the transcription of the axon guidance receptor Robo1 through a NF-κB binding element. In summary, our results reveal a mechanism by which spontaneous Ca^{2+} activity encodes a switch in the axon outgrowth program through the transcriptional regulation of Slit1 and Robo1 signaling.

As development proceeds, it appears necessary for axons approaching their targets to reduce their rate of extension to explore potential synaptic areas more thoroughly. This slowing down of growth can be achieved through either environmental cues or intrinsic signals[31,32]. In the thalamocortical system, we found that the progression of axons was slower when TCAs navigated through the cortex and that the steady decrease observed in their growth rate was a result of signals in the thalamus. Indeed, when isolated or placed into older host slices, early-phase thalamic axons kept growing faster than late-phase axons. These results are consistent with previous findings demonstrating an age-dependent loss in the ability of CNS neurons to grow axons[6,10], which occurs in discrete periods during embryonic or early postnatal development. Together, these observations reveal the existence of a critical time window after which neurons lose their ability to grow axons over long distances. Accordingly, the growth behavior of late thalamic axons was not reverted by V_m depolarization, a procedure that enhances axonal growth of early neurons.

Both *in vitro* and *in vivo* studies have shown that spontaneous activity is critical to ensure correct pathfinding and targeting of projecting neurons in the brain[16,33,34]. We found that, although the proportion of spiking cells increased as development proceeded, the frequency of Ca^{2+} transients diminished. Spontaneous activity is generally thought to increase during embryonic life[35–37]; however, developmental reductions in Ca^{2+} spike frequency have been observed in other systems[16,22,38], suggesting that changes in this activity might encode critical steps in neuronal maturation. Our findings provide evidence for a function of this change in spontaneous activity. Indeed, the initial phase of rapid TCA growth was correlated with high-frequency

Ca^{2+} transients, whereas attenuated TCA growth was concomitant with a reduction of this activity later in development. Our pharmacological studies revealed that, by increasing transients frequency, axon outgrowth was enhanced, whereas a decrease was associated with reduced axonal length. Complete suppression of activity was sufficient to prematurely attenuate the rate of axon elongation *in vitro* and *in vivo*. Our results therefore indicate that the developmental reduction in spontaneous thalamic activity intrinsically triggers a switch in the rate of TCA extension, supporting the idea that activity is instructive for axonal growth. Moreover, our observation that both reduction and suppression of spontaneous calcium activity resulted in similar phenotypes suggests that the amount of Ca^{2+} activity is the crucial factor.

The frequency of Ca^{2+} transients in *Xenopus* growth cones modulates axon growth, although in an opposite manner to that described here: growth cones with a high frequency of Ca^{2+} transients grow more slowly or retract, whereas those generating a lower frequency of transients advance more rapidly[20]. The changes that we observed likely consist of long-term modifications in activity-dependent control of axonal extension, whereas those reported in *Xenopus*[20] were almost immediate. Consistent with this, transient increase in electrical activity of hippocampal neurons induced growth cone stalling[39], suggesting that the mechanisms involved in fast regulation of axonal extension differ from those controlling the developmental state of the axon. Accordingly, even though late-stage axons were still able to grow at relatively high rates, they did not extend over long distances. Our observations are consistent with a nuclear response, leading to long-term modifications to the genetic program of the cell. This apparent discrepancy may reflect specific spatiotemporal characteristics of the downstream modifications observed, such that changes in intracellular Ca^{2+} concentration would activate different targets and generate diverse cellular responses. It will be interesting to determine whether rapid modifications in TCA motility also rely on transcriptional modifications.

Activity-dependent regulation of gene expression has been implicated in brain development[8], although until recently it was unclear whether this regulation occurs at the transcriptional level. We found that spontaneous activity repressed *Robo1* transcription, an effect that depended on regulatory sequences located upstream of the gene coding sequence. A recent study found that neurotransmitter specification relies on the activity-dependent regulation of the *tlx3* gene through a variant of the cAMP response element (CRE) motif in its promoter[17]. This CRE variant binds phosphorylated cJun, which in turn represses *tlx3* transcription. We found several motifs in the *Robo1* promoter that were putative targets for Ca^{2+}-sensitive transcription factors. Only the mutation of the NF-κB binding site 1 substantially decreased both the basal transcription of *Robo1* and its activity-dependent regulation, indicating that NF-κB might be a key transcription factor involved in Robo1-mediated growth. However, as this mutation did not completely abolish the activity-dependent regulation of *Robo1*, it is possible that atypical binding sites for NF-κB at the *Robo1* locus could maintain a regulatory activity or that other motifs for Ca^{2+}-dependent transcription factors, such as Oct-1 and NFAT, could also be implicated.

NF-κB has recently emerged as a major regulator of axon elongation[40] that either promotes or inhibits axon growth depending on the phosphorylation of specific residues in the NF-κB subunits. These opposite effects on axon growth have been recorded in the same population of neurons, but at distinct developmental stages[41], suggesting that a switch in the NF-κB signaling network might contribute to the observed axonal behavior. Among others, Ca^{2+} levels have been shown to modulate NF-κB activity[42], and the increase NF-κB activity triggered by the switch in calcium frequency occurring in late thalamic neurons could therefore lead to an increase of *Robo1* transcription and a decrease in TCA growth. However, the mechanism by which NF-κB transcriptional activity is regulated in thalamic neurons during the early and late phases of TCA growth remains to be elucidated. Moreover, we cannot exclude the possibility that the novo Robo1 protein synthesis might also be important for controlling TCA outgrowth, as it is accepted that *de novo* protein synthesis modulates axon guidance[43,44].

Our gain- and loss-of-function experiments revealed that altering Robo1 expression in thalamic neurons changed the rate of axon growth, suggest a role for the Robo1 receptors as a brake for TCA extension. Both pharmacological and genetic reduction of spontaneous activity augmented *Robo1* expression without affecting another member of the family, *Robo2*. Both *Robo1* mRNA and protein were upregulated during late embryonic development, mirroring changes in *Kir2.1* expression and suggesting that the natural increase in *Robo1* expression in the thalamus is mediated by activity-dependent mechanisms. Moreover, co-electroporation of a truncated form of Robo1 receptor with *Kir2.1* rescued the attenuation of TCA extension, suggesting that Robo1 is an important mediator of the effects of electrical activity on axon growth, although perhaps not the only one. Indeed, receptors of guidance cues that influence axon growth, such as Netrin 1 (ref. 2; E.M. and G.L.-B., unpublished observations) were also identified as genes that were affected by spontaneous activity. Thus, electrical activity may regulate axon growth by modifying the expression of distinct guidance receptors.

Our results show that in the *Robo1*$^{-/-}$ mouse there is a substantial increase in thalamic axon growth. This increase in axonal extension *in vivo* is consistent with that found in a *Robo1*$^{-/-}$ mouse in which exon 5 of the *Robo1* gene is missing[45]. As most TCAs express Robo1 and Robo2 receptors during outgrowth and pathfinding[46], we observed accelerated TCA growth in *Slit1*$^{-/-}$, and to a lesser extent in *Robo1*$^{-/-}$, embryos. The increased growth of wild-type axons in *Slit1*$^{-/-}$ slices *ex vivo* further supports a Slit1-dependent function of Robo1 in controlling TCA growth, although we cannot rule out the possibility that Robo1 might also promote outgrowth via homophilic binding[47]. In conclusion, our data have important implications for our understanding of how the brain is wired, and offer new perspectives that should be considered when contemplating axon regeneration and repair.

METHODS

Methods and any associated references are available in the online version of the paper.

Note: Supplementary information is available in the online version of the paper.

ACKNOWLEDGMENTS

We thank N. García and E. San Martin for outstanding technical assistance. We are also grateful to A. Nagy (Samuel Lunenfeld Research Institute) for the EGFP mice, M. Valdeolmillos (Instituto de Neurociencias de Alicante) for providing the calcium imaging set-up and helping with quantification of calcium activity in growth cones, F. Martini for advice on calcium imaging, G. Expósito for advice on two-photon imaging, O. Marín (Instituto de Neurociencias de Alicante) for reagents, M. Maravall for advice on data analysis, F. Viana (Instituto de Neurociencias de Alicante) for providing the inducible CHO-A1 cells, and M. Dominguez and A. Gontijo for access and advice on qPCR equipment. We are grateful to A. Nieto, P. Arlotta, E. Herrera and M. Valdeolmillos for advice and critical reading of the manuscript. We are also grateful to members of the López-Bendito laboratory and Herrera laboratory for stimulating discussions and comments. C.M. is recipient of a JAE-Predoctoral Fellowship from the CSIC. This work was supported by grants from the Spanish Ministerio de Ciencia e Innovacion (BFU2006-07138 to J.L. and BFU2009-08261 to G.L.-B.),

an Human Frontier Science Program Organization grant (RGP29/2008), the Consolider programme (CSD2007-00023) and an European Research Council grant (ERC-2009-StG_20081210 to G.L.-B.).

AUTHOR CONTRIBUTIONS

G.L.-B. conceived the idea. E.M. and G.L.-B. designed the study. E.M., C.M., E.L.-D. and G.L.-B. performed the *in vitro*, *ex vivo* and *in utero* electroporation experiments. E.L.-D. and L.B. performed the luciferase assays. A.V.P. performed the electrophysiological recordings. P.S. and S.G. performed the experiments on *Slit1* mutant mice. M.C.-P. performed the semiquantitative PCR and the collapse assay. M.J.L. performed the calcium recordings in CHO-A1 cells. S.P. subcloned the Kir2.1 plasmid. M.T.-L. produced the *Robo1*, *Robo2* and *Robo1; Robo2* mutant mice. J.G. supervised the luciferase assays. J.L. supervised the electrophysiological experiments. E.M., C.M. and G.L.-B. conducted the data analysis and wrote the paper.

COMPETING FINANCIAL INTERESTS

The authors declare no competing financial interests.

Published online at http://www.nature.com/doifinder/10.1038/nn.3160.
Reprints and permissions information is available online at http://www.nature.com/reprints/index.html.

1. López-Bendito, G. *et al.* Tangential neuronal migration controls axon guidance: a role for neuregulin-1 in thalamocortical axon navigation. *Cell* **125**, 127–142 (2006).
2. Métin, C., Deleglise, D., Serafini, T., Kennedy, T.E. & Tessier-Lavigne, M. A role for netrin-1 in the guidance of cortical efferents. *Development* **124**, 5063–5074 (1997).
3. Garel, S. & Rubenstein, J.L.R. Intermediate targets in formation of topographic projections: inputs from the thalamocortical system. *Trends Neurosci.* **27**, 533–539 (2004).
4. Braisted, J.E. *et al.* Netrin-1 promotes thalamic axon growth and is required for proper development of the thalamocortical projection. *J. Neurosci.* **20**, 5792–5801 (2000).
5. Tucker, K.L., Meyer, M. & Barde, Y. Neurotrophins are required for nerve growth during development. *Nat. Neurosci.* **4**, 29–37 (2001).
6. Blackmore, M. & Letourneau, P.C. Changes within maturing neurons limit axonal regeneration in the developing spinal cord. *J. Neurobiol.* **66**, 348–360 (2006).
7. Filbin, M.T. Myelin-associated inhibitors of axonal regeneration in the adult mammalian CNS. *Nat. Rev. Neurosci.* **4**, 703–713 (2003).
8. Spitzer, N.C. Electrical activity in early neuronal development. *Nature* **444**, 707–712 (2006).
9. Ming, G., Henley, J., Tessier-Lavigne, M., Song, H. & Poo, M. Electrical activity modulates growth cone guidance by diffusible factors. *Neuron* **29**, 441–452 (2001).
10. Goldberg, J.L. *et al.* Retinal ganglion cells do not extend axons by default: promotion by neurotrophic signaling and electrical activity. *Neuron* **33**, 689–702 (2002).
11. Fields, R.D., Neale, E. & Nelson, P. Effects of patterned electrical activity on neurite outgrowth from mouse sensory neurons. *J. Neurosci.* **10**, 2950–2964 (1990).
12. Gomez, T.M. & Zheng, J.Q. The molecular basis for calcium-dependent axon pathfinding. *Nat. Rev. Neurosci.* **7**, 115–125 (2006).
13. Tang, F., Dent, E.W. & Kalil, K. Spontaneous calcium transients in developing cortical neurons regulate axon outgrowth. *J. Neurosci.* **23**, 927–936 (2003).
14. Cohan, C.S. & Kater, S. Suppression of neurite elongation and growth cone motility by electrical activity. *Science* **232**, 1638–1640 (1986).
15. Borodinsky, L.N. *et al.* Activity-dependent homeostatic specification of transmitter expression in embryonic neurons. *Nature* **429**, 523–530 (2004).
16. Hanson, M.G. & Landmesser, L.T. Normal patterns of spontaneous activity are required for correct motor axon guidance and the expression of specific guidance molecules. *Neuron* **43**, 687–701 (2004).
17. Marek, K.W., Kurtz, L. & Spitzer, N. cJun integrates calcium activity and tlx3 expression to regulate neurotransmitter specification. *Nat. Neurosci.* **13**, 944–950 (2010).
18. López-Bendito, G. & Molnár, Z. Thalamocortical development: how are we going to get there? *Nat. Rev. Neurosci.* **4**, 276–289 (2003).
19. Skaliora, I., Adams, R. & Blakemore, C. Morphology and growth patterns of developing thalamocortical axons. *J. Neurosci.* **20**, 3650–3662 (2000).
20. Gomez, T.M. & Spitzer, N.C. *In vivo* regulation of axon extension and pathfinding by growth-cone calcium transients. *Nature* **397**, 350 (1999).
21. Burrone, J., O'Byrne, M. & Murthy, V.N. Multiple forms of synaptic plasticity triggered by selective suppression of activity in individual neurons. *Nature* **420**, 414–418 (2002).
22. Demarque, M. & Spitzer, N.C. Activity-dependent expression of Lmx1b regulates specification of serotonergic neurons modulating swimming behavior. *Neuron* **67**, 321–334 (2010).
23. Mizuno, H., Hirano, T. & Tagawa, Y. Evidence for activity-dependent cortical wiring: formation of interhemispheric connections in neonatal mouse visual cortex requires projection neuron activity. *J. Neurosci.* **27**, 6760–6770 (2007).
24. Itoh, K., Ozaki, M., Stevens, B. & Fields, R. Activity-dependent regulation of N-cadherin in DRG neurons: differential regulation of N-cadherin, NCAM, and L1 by distinct patterns of action potentials. *J. Neurobiol.* **33**, 735–748 (1997).
25. Dolmetsch, R.E., Lewis, R.S., Goodnow, C.C. & Healy, J.I. Differential activation of transcription factors induced by Ca^{2+} response amplitude and duration. *Nature* **386**, 855–858 (1997).
26. Fajardo, O., Meseguer, V., Belmonte, C. & Viana, F. TRPA1 channels: novel targets of 1,4-dihydropyridines. *Channels (Austin)* **2**, 429–438 (2008).
27. Sugiyama, C. *et al.* Activator protein-1 responsive to the group II metabotropic glutamate receptor subtype in association with intracellular calcium in cultured rat cortical neurons. *Neurochem. Int.* **51**, 467–475 (2007).
28. Xiang, G. *et al.* Identification of activity-dependent gene expression profiles reveals specific subsets of genes induced by different routes of Ca^{2+} entry in cultured rat cortical neurons. *J. Cell. Physiol.* **212**, 126–136 (2007).
29. Bagri, A. *et al.* Slit proteins prevent midline crossing and determine the dorsoventral position of major axonal pathways in the mammalian forebrain. *Neuron* **33**, 233–248 (2002).
30. Stein, E. & Tessier-Lavigne, M. Hierarchical organization of guidance receptors: silencing of netrin attraction by slit through a Robo/DCC receptor complex. *Science* **291**, 1928–1938 (2001).
31. Sann, S.B., Xu, L., Nishimune, H., Sanes, J.R. & Spitzer, N.C. Neurite outgrowth and *in vivo* sensory innervation mediated by a Ca(V)2.2-laminin beta 2 stop signal. *J. Neurosci.* **28**, 2366–2374 (2008).
32. Porter, B.E., Weis, J. & Sanes, J.R. A motoneuron-selective stop signal in the synaptic protein S-laminin. *Neuron* **14**, 549–559 (1995).
33. Butler, A.K., Dantzker, J., Shah, R. & Callaway, E. Development of visual cortical axons: layer-specific effects of extrinsic influences and activity blockade. *J. Comp. Neurol.* **430**, 321–331 (2001).
34. Uesaka, N., Hayano, Y., Yamada, A. & Yamamoto, N. Interplay between laminar specificity and activity-dependent mechanisms of thalamocortical axon branching. *J. Neurosci.* **27**, 5215–5223 (2007).
35. Nishimaru, H., Iizuka, M., Ozaki, S. & Kudo, N. Spontaneous motoneuronal activity mediated by glycine and GABA in the spinal cord of rat fetuses *in vitro*. *J. Physiol. (Lond.)* **497**, 131–143 (1996).
36. Scain, A.L. *et al.* Glycine release from radial cells modulates the spontaneous activity and its propagation during early spinal cord development. *J. Neurosci.* **30**, 390–403 (2010).
37. Picken Bahrey, H.L. & Moody, W.J. Early development of voltage-gated ion currents and firing properties in neurons of the mouse cerebral cortex. *J. Neurophysiol.* **89**, 1761–1773 (2003).
38. Xiao, Q., Xu, L. & Spitzer, N.C. Target-dependent regulation of neurotransmitter specification and embryonic neuronal calcium spike activity. *J. Neurosci.* **30**, 5792–5801 (2010).
39. Ibarretxe, G., Perrais, D., Jaskolski, F., Vimeney, A. & Mulle, C. Fast regulation of axonal growth cone motility by electrical activity. *J. Neurosci.* **27**, 7684–7695 (2007).
40. Gutierrez, H. & Davies, A.M. Regulation of neural process growth, elaboration and structural plasticity by NF-kappaB. *Trends Neurosci.* **34**, 316–325 (2011).
41. Gutierrez, H., O'Keeffe, G.W., Gavalda, N., Gallagher, D. & Davies, A.M. Nuclear factor kappa B signaling either stimulates or inhibits neurite growth depending on the phosphorylation status of p65/RelA. *J. Neurosci.* **28**, 8246–8256 (2008).
42. Riquelme, D. *et al.* High-frequency field stimulation of primary neurons enhances ryanodine receptor–mediated Ca^{2+} release and generates hydrogen peroxide, which jointly stimulate NF-kappaB activity. *Antioxid. Redox Signal.* **14**, 1245–1259 (2011).
43. Tcherkezian, J., Brittis, P.A., Thomas, F., Roux, P.P. & Flanagan, J.G. Transmembrane receptor DCC associates with protein synthesis machinery and regulates translation. *Cell* **141**, 632–644 (2010).
44. Jung, H., Yoon, B.C. & Holt, C.E. Axonal mRNA localization and local protein synthesis in nervous system assembly, maintenance and repair. *Nat. Rev. Neurosci.* **13**, 308–324 (2012).
45. Andrews, W. *et al.* Robo1 regulates the development of major axon tracts and interneuron migration in the forebrain. *Development* **133**, 2243–2252 (2006).
46. López-Bendito, G. *et al.* Robo1 and Robo2 cooperate to control the guidance of major axonal tracts in the mammalian forebrain. *J. Neurosci.* **27**, 3395–3407 (2007).
47. Zallen, J.A., Yi, B.A. & Bargmann, C.I. The conserved immunoglobulin superfamily member SAX-3/Robo directs multiple aspects of axon guidance in *C. elegans*. *Cell* **92**, 217–227 (1998).

ONLINE METHODS

Mouse strains. The wild-type and GFP-expressing mice used in this study[48] were on a CD1 background. *Robo1*$^{-/-}$*; Robo2*$^{-/-}$ double-mutant embryos were obtained by crossing *Robo1*$^{+/-}$*; Robo2*$^{+/-}$ adult mice on a CD1 background, whereas *Robo2*$^{-/-}$ mice[46,49] and the *Slit1*$^{-/-}$ colony[29] were maintained on a C57BL/6 background. Genotyping was performed by PCR as described previously[46,49,50] and the day of the vaginal plug was considered as E0.5. All animal procedures were approved by the Committee on Animal Research at the University Miguel Hernández and were carried out according to Spanish and European Union regulations.

***In utero* electroporation.** Pregnant females (E12.5) were deeply anesthetized with isofluorane to perform laparotomies and the embryos were visualized through the uterus with a fiber-optic light source. The following DNA fragments were subcloned into pCAGG plasmids and used for *in utero* electroporation at a concentration of 1.5 μg μl^{-1}: *Kir2.1-IRES-Gfp*, mutant *Kir2.1-IRES-Gfp* (both generous gifts from V. Murthy, Harvard University), full-length *Robo1* and *Robo1*Δ*C* (both generous gifts from Genentech). All plasmids were co-electroporated with a plasmid encoding *Gfp* at 0.9 μg μl^{-1} and mixed with 1% fast green (vol/vol, Sigma), and they were injected into the third cerebral ventricle of each embryo through a glass capillary. For electroporation, the negative and positive palettes were placed near the head of the embryo, and five square electric pulses of 35 V and 50 ms were delivered through the uterus, at 950-ms intervals, using a square pulse electroporator CUY21 Edit (NepaGene). The surgical incision was then closed and embryos were allowed to develop until E15.5, at which point they were removed, fixed in 4% paraformaldehyde (PFA, vol/vol) and analyzed.

Axon tracing and immunohistochemistry. For axon tracing, embryonic brains or cultured slices were fixed in 4% PFA overnight or for 30 min, respectively. Small DiI crystals (1,1′-dioctadecyl 3,3,3′,3′-tetramethylindocarbocyanine perchlorate, Molecular Probes) were inserted into the thalamus and allowed to diffuse for 1–3 weeks at 37 °C before vibratome sections (100 μm) were obtained. Hoechst (Sigma) was used to counterstain the nuclei. For immunohistochemistry, cultured slices and explants were fixed in 4% PFA for 30 min and in mouse embryos for 2–3 h. The following antibodies were used: mouse antibody to βIII tubulin (1:1,000, MMS-435P, Covance), rabbit antibody to GFP (1:1,000, A-11122, Invitrogen), chicken antibody to GFP (1:3,000, GFP-1020, Aves Labs), rabbit antibody to calretinin (1:1,000; 7699/4, Swant), goat antibody to Robo1 (1:20, AF1749, R&D Systems), goat antibody to mouse Alexa-546 (1:500, A11003, Molecular Probes), donkey antibody to rabbit Alexa-488 (1:500, A21206, Molecular Probes), goat antibody to rabbit Alexa 594 (1:500, A11012, Molecular Probes), goat antibody to chicken Alexa-488 (1:500, A11039, Molecular Probes), donkey antibody to goat Alexa-546 (1:500, A11056, Molecular Probes).

Culture experiments, *in vitro* electroporation and pharmacological studies. Organotypic slices of embryonic mice were prepared and cultured for 48 h as described previously[1]. For isochronic and heterochronic transplantation experiments, brains were cut 45° to the sagittal plane to obtain host slices in which the entire thalamocortical pathway is maintained[51]. Wild-type thalamic explants from intermediate rostro-caudal levels of the thalamus were selected and transplanted into wild-type or *Slit1*$^{-/-}$ host coronal slices. Normalized fluorescence was measured using ImageJ at a distance of 1–300 μm from the border of the explant or 301–1,200 μm from the border of the explant. For axon outgrowth assays, thalamic explants from coronal slices of wild-type and mutant mice were dissected out and plated on coverslips coated with poly-L-lysine (0.1 mg ml^{-1}, Sigma) and laminin (20 mg ml^{-1}, Sigma). To test the effect of electrical silencing in thalamic neurons *in vitro*, focal electroporation of coronal brain slices was performed as described previously[1]. The following DNA plasmids were used at a concentration of 1.2 μg μl^{-1}: *Kir2.1-IRES-Gfp*, mutant *Kir2.1-IRES-Gfp*, *dsRed* and an empty plasmid. All plasmids were co-electroporated with a plasmid encoding *Gfp* at 0.9 μg μl^{-1} and mixed with 1% fast green (Sigma). For pharmacological studies, KCl (2.5 to 10 mM) or nifedipine (10 μM), ω-conotoxin GVIA (1 μM, Tocris) or 5 nM Slit1 (R&D Systems) were added to the culture medium at the time of plating.

Time-lapse imaging and calcium recordings. For time-lapse imaging, thalamic explants from GFP-expressing embryos were prepared as described above, cultured in glass bottom micro-well dishes (MatTek) overnight and placed on a heated (37 °C) microscope stage to be visualized on a confocal Leica inverted microscope. Calcium imaging was performed in thalamocortical slices or growth cones from thalamic explants loaded with either Oregon Green BAPTA-AM (Molecular Probes) with pluronic acid (0.01%, vol/vol) for 1–2 h or after retrograde labeling with Oregon Green injected in the internal capsule. Slices or explants were placed in a recording chamber of an upright Leica DMFLSA stage, perfused with warmed artificial cerebrospinal fluid (124 mM NaCl, 4 mM KCl, 2.4 mM $CaCl_2$, 1.3 mM $MgSO_4$, 1.25 mM KH_2PO_4, 26 mM $NaHCO_3$ and 10 mM glucose) bubbled with 95% O_2 with 5% CO_2. For pharmacological studies, $NiCl_2$ (50 μM) or recombinant Slit1 protein (5 nM) were added in the perfusing artificial cerebrospinal fluid medium. Slices or explants were excited at 488 nm with a Mercury arc lamp. Images were acquired every 0.33 Hz with a cooled CCD Orca camera (Hamamatsu) controlled by the AquaCosmos software (Hamamatsu).

Electrophysiology. Thalamic cells were visualized through a 40× water immersion objective. Neurons electroporated with *Kir2.1* and *Gfp* or *Gfp* alone were identified by fluorescence using an upright fluorescence microscope (Olympus BX50WI); all experiments were performed at 22–25 °C. The slices were continuously perfused with an external bath solution (containing 124 mM NaCl, 3 mM KCl, 1.25 mM KH_2PO_4, 1 mM $MgCl_2$, 2 mM $CaCl_2$, 26 mM $NaHCO_3$, and 10 mM glucose: 300 mOsm, pH 7.3) and continuously oxygenated with 95% O_2 and 5% CO_2. Glass micropipettes had a resistance 5–7 MΩ and they were filled with an internal solution of KCl (130 mM KCl, 5 mM NaCl, 0.4 mM $CaCl_2$, 1 mM $MgCl_2$ and 10 mM HEPES, (290 mOsm, pH 7.3) or 140 mM potassium gluconate, 4 mM NaCl, 0.3 mM EGTA, 10 mM HEPES, 2 mM Mg-ATP and 0.5 mM GTP (290 mOsm, pH 7.3)). Pipettes were lowered onto individual cells and maintained at constant positive pressure. The pressure was then released after touching the cell and a Gigaseal was established. A holding potential of −60 mV was applied, and brief pulses of suction were applied until the plasma membrane inside the pipette ruptured. Recordings were made using an Axopatch 200 amplifier (Molecular Devices). Resting membrane potential (V_r) was measured immediately after establishing the whole-cell configuration.

Quantitative and semiquantitative PCR. Total RNA from electroporated thalamic explants cultured for 60 h was extracted using the RNeasy Kit (Qiagen). RNA was treated with RNase-free DNaseI for 30 min at 37 °C before reverse transcribing the RNA for 1 h at 42 °C into single-stranded cDNA using SuperScript II Reverse Transcriptase and Oligo(dT)$_{12–18}$ primers (Invitrogen). qPCR was carried out on an Applied Biosystems 7300 real-time PCR unit using the Power SYBR Green PCR Master Mix (Applied Biosystems), 5 μl of cDNA and the appropriate primers. Each independent sample was assayed in duplicate and gene expression was normalized to that of *Gapdh*. The following sequences of primers were used for semiquantitative PCR: *Kir2.1*^{346} (forward TTTGGGAACGGGAAGAGTAAAGTC and reverse TTTTTGGCTGTGTGTTTTGG); *Kir2.1*^{134} (forward TTTTTGGCTGTGT GTTTTGG and reverse GGTTGTCTGGGTCTCAATGG); *Robo1*^{155} (forward CGCAAGAAGAGAAACGGACTC and reverse TGCGTGGCAGGTTCA CTAATG); *Robo1*^{232} (forward TTCAGCATCTGGCTTTACAG and reverse AGCAGTCATTGTGGTTGTT); *Robo2* (forward CCAAGAAGAAACTCGG AAAGC and reverse ATTTGAGCCCACATATCCAAT); and *Gapdh* (forward AAAATGGTGAAGGTCGGTGT and reverse CTCACCCCATTTGATGT TAG). For qPCR, the following set of primers were used: *Gapdh* (forward CGG TGCTGAGTATGTCGTGGAGT and reverse CCAAGAAGAAACTCGG AAAGC); *Robo1* (forward AGGGAAGCCTACGCAGATG and reverse TGG ACAGTGGGCGATTTTAT); *Robo2* (forward GAGAATCGGGTGGGAA AAGT and reverse CACAAACTGTGGAGGAGCAA); and *Kir2.1* (forward GTGT CCGAGGTCAACAGCTT and reverse GGTTGTCTGGGTCTCAATGG).

Primary thalamic cell culture, cell lines and transfection. For primary thalamic neurons culture mice were killed and embryos were extracted. After brain dissection, thalami were removed and collected in Krebs, and then trypsinized and dissociated with a fire-polished Pasteur pipette to finally plate 200,000–300,000 cells per well in a 12-well plate in plating medium. Primary thalamic cells were cultured in maintenance medium at 37 °C with 5% CO_2 carefully replacing the medium every 2 d. Cells were transfected using Amaxa Basic Nucleofector Kit (Lonza).

An inducible CHO cell line stably expressing mouse TRPA1 channels (CHO-A1) was kindly provided by F. Viana. CHO-A1 cells were cultured in DMEM

containing 10% fetal bovine serum (vol/vol), 2% glutamax (vol/vol, Invitrogen), 1% non-essential amino acids (vol/vol, Invitrogen), 200 μg ml^{-1} penicillin/streptomycin, 5 μg ml^{-1} Blasticidin (Invitrogen) and 800 μg ml^{-1} hygromycin (Sigma). Expression of TRPA1 was induced by application of 0.25 μg ml^{-1} tetracycline. SH-SY5Y cells were routinely cultured in DMEM containing 10% fetal bovine serum, 1% glutamax (Invitrogen) and 100 μg ml^{-1} penicillin/streptomycin. Cells were transfected using Fugene HD (Promega).

Luciferase assays. CHO-A1 cells plated in 24-well plates were co-transfected with 200 ng of a luciferase reporter plasmid, 50 ng of pRL-TK and 250 ng of pCAGG empty vector, or 50 ng of *Kir2.1-IRES-Gfp* and 200 ng of pCAGG. TRPA1 channel expression was induced by application of 0.25 μg ml^{-1} tetracycline 36 h after transfection. The cells were lysed 12 h later and luciferase activity was measured using a Dual Luciferase Reporter Assay kit (Promega) according to the manufacturer's guidelines. Each sample was assayed in triplicate and luminescence was measured on a Sirius luminometer (Berthold DS). The ratio of pGL3-based luciferase reporter activity to pRL-TK luciferase activity was used to determine the true reporter activity.

Molecular cloning and genomic analysis. Bioinformatic searches in the mouse *Robo1* gene were performed using the Ensembl Genome Browser (http://www.ensembl.org/index.html). A 2,446-bp fragment of the mouse *Robo1* gene was amplified from mouse brain genomic DNA using the primers PromoterRobo1 F (5′-CTGCACGTTTCTTGTTTTTACTG) and PromoterRobo1 R (5′-GGACCAGCGAAAGAGATGAA). This fragment was cloned into the pCR-Blunt II-TOPO using the Zero Blunt TOPO PCR Cloning Kit (Invitrogen) and subsequently into the pGL3-Basic Vector (Promega). The TFSEARCH (http://www.cbrc.jp/research/db/TFSEARCH.html) and MATCH (http://www.bioinfo.de/isb/gcb01/poster/goessling.html) bioinformatics tools were used to search for putative transcription factor binding sites in the 2,446-bp Robo1 promoter sequence. The ECR Browser (http://ecrbrowser.dcode.org/) was used with the default settings (100 bp, 70% identity) to identify conserved regions in the *Robo1* promoter. Mutations in the NF-kB and AP-1 binding sites were introduced by site-directed mutagenesis giving rise to the following sequence substitutions: TTGGGAG to TTCCTAG (NF-kB site 1), GGGGAAA to GGCCCAA (NF-kB site 2) and TGACTCA to TGGTGCA (AP-1 site).

Quantification of axon growth and statistical analysis. ImageJ software was used for image processing and to analyze axon length *in vitro* and *in vivo*. To quantify axon growth in thalamic explants, the 40 longest axons in each explant were analyzed using the NeuronJ plug-in. To quantify the cortical extension of TCAs labeled *in utero*, only brains with a similar degree of electroporation in the thalamus were selected for analysis. Slices (60 μm) were obtained and images of the cortex were sampled at two different rostro-caudal levels (rostral and intermediate, three sections for each level and brain). A horizontal line was drawn from the edge of the pallial-subpallial boundary at the ventricle of each slice. The cortical area delimited by this line was then linearized using the Straighten plug-in of the ImageJ software. In this area, the distance covered by labeled axons was measured and normalized to the total length of the region defined. For quantification of axonal speed of growth *ex vivo*, the thalamus of oblique thalamocortical slices from E13.5 and E15.5 brains were electroporated with GFP. After 24 to 48 h, time-lapse imaging was performed using two-photon microscope for periods of recording of 4 to 12 h and an acquisition interval of 15 min. The speed of growth of each axon in identified forebrain structures was determined using the Manual tracking plug-in of the ImageJ software. Statistical analysis was performed using Prism software 5.0 (GraphPad).

48. Hadjantonakis, A.K., Gertsenstein, M., Ikawa, M., Okabe, M. & Nagy, A. Generating green fluorescent mice by germline transmission of green fluorescent ES cells. *Mech. Dev.* **76**, 79–90 (1998).
49. Andrews, W. *et al.* The role of Slit-Robo signaling in the generation, migration and morphological differentiation of cortical interneurons. *Dev. Biol.* **313**, 648–658 (2008).
50. Long, H. *et al.* Conserved roles for Slit and Robo proteins in midline commissural axon guidance. *Neuron* **42**, 213–223 (2004).
51. Agmon, A. & Connors, B.W. Thalamocortical responses of mouse somatosensory (barrel) cortex *in vitro*. *Neuroscience* **41**, 365–379 (1991).

doi:10.1038/nn.3160